A semi-anthropomorphic breast phantom with tunable blood oxygenation levels for use in quantitative photoacoustics

Maura Dantuma*, Javier Ortega Julia, and Srirang Manohar

***Abstract*—Photoacoustic imaging is an upcoming technique with potential in breast cancer screening and diagnosis. It is able to visualize the breast's vasculature. Its quantitative counterpart, called quantitative photoacoustics, potentially enables the derivation of local blood oxygen saturations when two or more optical wavelengths are used. Tumors can potentially be detected by looking at abnormal vessel shapes, high vascular densities or regions with a low oxygenation. In order to obtain accurate oxygen saturation estimations with quantitative photoacoustics, realistic light propagation models are required. Several models are available, but it is difficult to check their validity on real breasts due to the unknown ground truths, while simple objects having known ground truths are known to overestimate the performance of the algorithms. Therefore, measurements on an object that mimics the breast both optically as well as acoustically, and which has a complex but known morphology, are therefore required. We have previously reported on the first semi-anthropomorphic photoacoustic-ultrasound breast phantom. In this work, we build further upon this to make it suitable for use in quantitative photoacoustics. We demonstrate a method to embed blood vessels and tumors into the phantom where blood with a controlled oxygenation level can be flushed through.**

***Index Terms*—Breast imaging, photoacoustics, quantitative photoacoustics**

I. Introduction

BREAST cancer is one of the most leading causes of deaths in women. In 2018, 2.088.849 new cases of breast cancer were diagnosed and 626.679 women worldwide died of breast cancer that same year [1]. The increase in breast cancer cases in the United States in the 1980s, followed by a decrease in mortality of 34% from 1990 to 2010, has been thought to be partially attributable to early detection as a result of the rapid introduction of X-ray mammography (MMG) screening [2], [3]. While there is not consensus as yet specifically about the advantages of X-ray mammography in this respect, it is generally accepted that early detection of breast cancer is of great importance. It is also generally accepted that currently used imaging modalities have many drawbacks and lead to cancers still being missed and benign abnormalities often being perceived as malignancies [4]–[6]. This is why the search for new breast imaging techniques is still ongoing.

All authors are from the Biomedical Photonic Imaging (BMPI) group, and the Multi-Modality Medical Imaging (M3I) group of the TechMed Centre, University of Twente, Enschede, The Netherlands.

*correspondence address: m.dantuma@utwente.nl

This work was part of the European Horizon 2020 PAMMOTH project under grant agreement No 732411, an initiative of the Photonics Public Private Partnership.

Photoacoustic (PA), or optoacoustic, imaging is one of the upcoming technologies for use in breast cancer screening and/or diagnosis and has shown to be able to non-invasively visualize blood vessels inside the breast [7]–[10]. PA imaging is based on the photoacoustic effect which converts time-variant optical energy into acoustic waves, via the physical phenomenon of thermo-elastic expansion [11]–[13]. During a measurement, the object of interest is illuminated with pulsed laser light, which gets scattered by the tissue and will be specifically absorbed by tissue chromophores. The photoacoustically generated US waves can be detected outside of the breast with US detectors [11]–[13]. A chromophore that is of high interest in PA breast imaging is hemoglobin (Hb), a protein in the blood that gives blood its red color [14]. PA signals will be generated in the blood due to the high absorption contrast of Hb, and images of the blood vessels inside the breast can be reconstructed [12]. Tumors are known to have an abnormal vessel network. Vessels are heterogeneous, tortuous and they branch chaotically. The blood vessel density is also known to be high due to the process called angiogenisis [15]. These deviations from healthy vasculature are potential hallmarks to identify cancer.

Arguably the most interesting application of PA is its ability to derive quantitative information about local chromophore concentrations, when the tissue is illuminated with two or multiple wavelengths [16]. The oxygen saturation (sO_2) of the blood can be derived from the concentrations of Hb and its oxygenated version HbO_2, that have differences in their absorption spectra [16], [17]. Regions with a low sO_2 may be an extra indication for the presence of a tumor, since tumors have a high metabolism and thereby use more oxygen than usual. Besides, the leaky and tortuous vessels are inefficient in transporting oxygen rich blood to the tumor site [15].

The concentration of both chromophores can be derived from the measured PA spectra, if the local optical fluence is known. Different light propagation models are developed and used to approximate this, but they will always give an estimation due to the unknown complexity of the breast and the wavelength dependency of tissue optical properties [16], [18].

Several test-objects with known optical and acoustic properties have been developed for use in QPAT to e.g. investigate the accuracy of the light propagation models [19]–[22], [22]. An example is an oxygen-tunable cubic shaped phantom with blood-filled channels [22] that was used to investigate the depth-dependency of sO_2 estimations.

978-1-7281-1895-6/19/$31.00

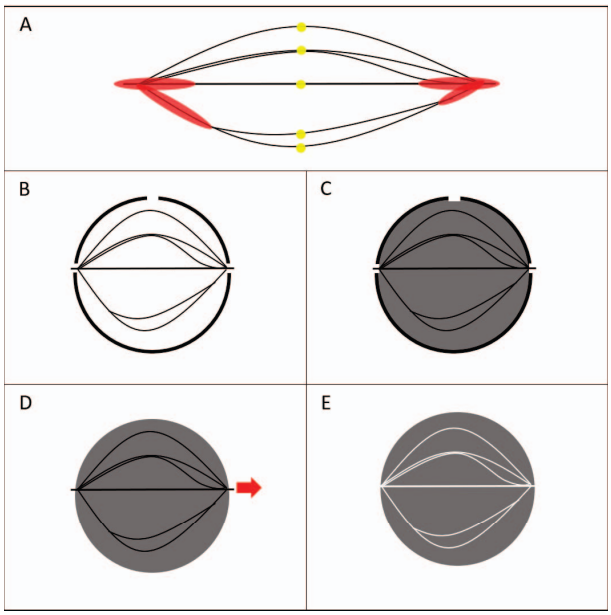

Fig. 1. A: Wire network showing soldering points, in red, strong soldering to create bifurcations and common inlet and outlet; in yellow, weak soldering that will be broken when pulling out. B: Tumor mold with the wires on it. C: Mold is filled with PVCP. D: Mold is removed and wires are pulled out. E: Tumor phantom with channels is ready.

In this work we go a step further, and develop semi-anthropomorphic phantom with tissue realistic optical and acoustic properties and a morphological complexity that approximates a real breast, such that the algorithms are challenged to the same order as in real breasts. This phantom will be a valuable tool in bridging the gap between laboratory experiments and clinical studies. In previous work we have already shown a method to develop a semi-anthropomorphic PA breast phantom from polyvinylplastisol (PVCP) formulations [23], [24]. Blood vessels embedded in this phantom were solid and the wavelength independency of the vessels did not allow to use the phantom for QPAT. In this work we build further upon this protocol and take the first steps to change the blood vessel structures into hollow channels such that blood can be flushed through and such that the phantom can be used in QPAT. We demonstrate the appearance of the vessels in US imaging and MRI imaging.

II. Materials and Methods

The protocol for developing a semi-anthropomorphic PA breast phantom containing skin, fat, fibroglandular and blood mimicking materials (MM) with tissue relevant optical and acoustic properties was described in Refs. [23], [24]. The phantom was made from custom PVCP forumulations, inspired by the work of Vogt *et al.* [25], [26]. The morphology was partially based on MRI-segmented tissue volumes [27] to give it a realistic shape. Molds were designed based on these volumes, to pour the PVCP into and to give the phantom the realistic shape. The embedded blood vessels were made from PVCP doped with black plastic coloring (BPC), to increase the optical absorption. In this work, the PVCP blood vessels and tumors are replaced by hollow channels of varying diameters, filled with pig blood, that are connected to a flow-system to oxygenate and pump the blood through the phantom [22]. Two vessel networks both containing one tumor were embedded in the phantom. One located in the fat layer and the other in the fibroglandular layer, to have vessels located at various depths inside the phantom.

A. Hollow channels

An approximation to a realistic blood vessel network was developed and embedded in the phantom. Flow channels were developed by placing copper wires in the mold before pouring PVCP. After pouring, the PVCP solidified around the wires and, the wires were pulled out to remain with hollow channels. Wires with 0.5, 1 and 1.5 mm diameters were used to simulate the different sizes of blood vessels. Wires were partially soldered together to create bifurcations and to merge all ends to create a single blood inlet and outlet to connect the phantom to the flow-system, see red highlighted parts in Figure 1 A. To ensure that the wires could be pulled off after PVCP cooling, the wires were cut in the middle and soldered again, to create a weak point that will break when pulling, to remove the entire copper network from the phantom. These soldering points are depicted in yellow in Figure 1 A.

Two of these vessel networks were developed, one consisting of seven wires to include in the fat layer of the phantom and one made from six wires to include in the fibroglandular layer.

B. Tumor models

The dense network of microvessels inside the tumor developed by angiogenisis could not be mimicked due to its microscopic size and complexity. Larger vessels present inside tumors that can be considered as feeding vessels could be included. To develop the tumor models, a 2 cm diameter spherical mold, having two holes on top and two on the sides was 3D printed from polylactic acid (PLA). Five 0.5 mm and one 1.5 mm metal wire were placed through the two side holes (They were not soldered, as the lateral holes held them together) (see Figure 1 B), and the mold was filled through one of the top holes with fibroglandular tissue mimicking PVCP that was doped with BPC to mimick the enhanced optical absorption by the microvasculature (see Figure 1 C). The second hole in the top was designed for letting the air out. The BPC increased the μ_a from 0.3 cm^{-1} to 0.6 cm^{-1}, which is in correspondence with literature which tells that the μ_a in tumors is a factor two to four higher than in healthy breast tissue [28]–[30]. The tumor was removed from the mold and the wires were pulled out from one of the sides after the solidification of the PVCP (see Figure 1 D). Then, the tumor is left with the hollow channels inside (see Figure 1 E).
After cutting the copper wires representing the breast vasculature (yellow dots, Figure 1 A), one of the open ends was stringed through the 1.5 mm channel in the tumor. After this, the wires were soldered together as described above. In this way, the tumor was connected to the vessel network.

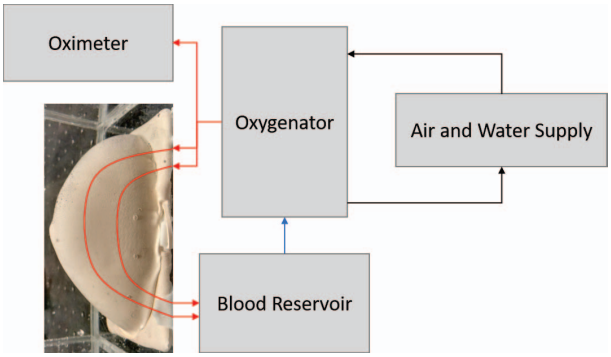

Fig. 2. Flow system for the breast phantom including the oxygenator, an oximeter, the phantom, a blood reservoir and the water and air inputs needed by the oxygenator

Fig. 3. Final semi-anthropomorphic photoacoustic breast phantom embedded with blood vessel mimics.

C. Flow system

To let the blood flow through the hollow channels in the phantom, a closed flow system was designed (see Figure 2) based on [22]. This system contains a membrane oxygenator (MINIMAX PLUS, Hollow Fiber Oxygenator, Medtronics), that is connected to air and water flows, to regulate the blood temperature and oxygenation. A peristaltic pump (Opencircuit.nl, The Netherlands) pumps the (deoxygenated) blood from the reservoir into the oxygenator, oxygenated blood enters the phantom and exits again in the reservoir, closing the cicle. In addition, some blood can be collected from the output of the oxygenator in order to measure its oxygen saturation using a commercial oximeter (AVOXimeter 1000E, ITC)

D. Imaging

The phantom was imaged with B-mode US and MRI to investigate whether all channels are functional and to digitize their locations. US B-scans were made with the Alpinion E-Cube12a research system (Alpinion Medical Systems, Korea) using the SC1-4H probe operating at 4 MHz, the channels of the phantom were filled with air, to make them highly reflective and localize them easily. MRI images were acquired with a 0.25 Tesla G-Scan Bio system (Esaote Benelux B.V.) utilizing a HYCE sequence, two scans were taken, one with air in the channels and the second with the channels filled with water to act as a contrast agent, if a channel is found to have water, then we can assume it is connected to the network, otherwise, the channel is closed at some point and is not viable.

III. Results

Figure 3 shows a photograph of the phantom after the phantom production process. The photograph shows the end result from the top side. This phantom contained the soldered network with one tumor model on it, placed just above the silicon skin layer that was produced according to the protocol in [23], [24]. A second soldered network is placed on top of the PVCP fat MM layer. The phantom is finally topped off with fibroglandular tissue mimicking PVCP. The phantom was then imaged with US (Figure 4) and MRI (Figure 5) to check the viability and connectivity of the channels.

IV. Discussion and Outlook

The US image shows some of the air-filled channels (red arrows) and both of the tumors (yellow circles), one in the fat layer, more superficial; and the second one in the fibroglandular layer, more deep. The boundary between the fat (darker) and fibroglandular (lighter) layer can also be observed due to the difference in speckle contrast.

To further study the channels and their connectivity, the MR scan in Figure 5 show a transverse view of the phantom (left). With the used imaging sequence, water lights up white. The sagittal plane (right), shows longitudinal white channels, including a channel that goes through the tumor (darker circle in the outer layer). The presence of water in the channels implies that they are connected. One of the channels was seen as black, meaning that it is not connected to the network. Within the visible tumor in the MR image, just the big channel (1.5 mm) is seen as white, this can imply that the smaller channels (0.5 mm) are not present, not connected or not filled. If they are not filled, it can be explained by the low water pressure, that will prevent it from going inside smaller channels when bigger ones are present.

These images show the viability of most of the blood vessels included in the breast phantom, they also confirm that the tumors and the different layers can be seen with US imaging. Future experiments will image the phantom with QPAT while flushing pig blood through the channels and changing the blood oxygenation.

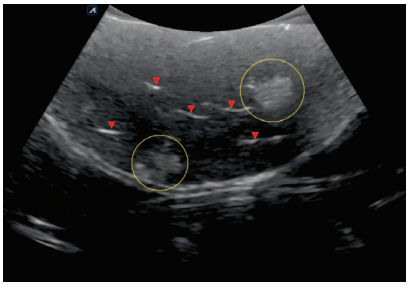

Fig. 4. Ultrasound scan of breast phantom. Red arrows point towards blood channels and yellow circles mark the tumors.

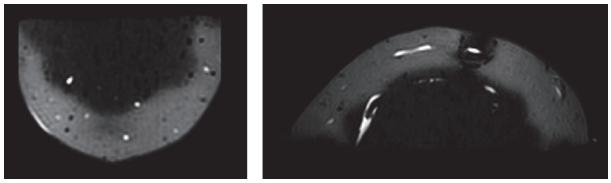

Fig. 5. 3D slices of the MR scan of the breast phantom, white areas represent the water inside the hollow channels. Left is the transverse view and right sagittal view.

ACKNOWLEDGEMENTS

The authors thank Dr. Frank Simonis for helping in acquiring the MRI images. This work was part of the European Horizon 2020 PAMMOTH project under grant agreement No 732411, an initiative of the Photonics Public Private Partnership.

REFERENCES

[1] F. Bray, J. Ferlay, I. Soerjomataram, R. L. Siegel, L. A. Torre, and A. Jemal, "Global cancer statistics 2018: Globocan estimates of incidence and mortality worldwide for 36 cancers in 185 countries," *CA: a cancer journal for clinicians*, vol. 68, no. 6, pp. 394–424, 2018.

[2] C. DeSantis, J. Ma, L. Bryan, and A. Jemal, "Breast cancer statistics, 2013," *CA: a cancer journal for clinicians*, vol. 64, no. 1, pp. 52–62, 2014.

[3] R. L. Siegel, K. D. Miller, and A. Jemal, "Cancer statistics, 2016," *CA: a cancer journal for clinicians*, vol. 66, no. 1, pp. 7–30, 2016.

[4] R. J. Hooley, L. Andrejeva, and L. M. Scoutt, "Breast cancer screening and problem solving using mammography, ultrasound, and magnetic resonance imaging," *Ultrasound Quarterly*, vol. 27, no. 1, pp. 23–47, 2011.

[5] W. A. Berg, "Supplemental screening sonography in dense breasts," *Radiologic Clinics*, vol. 42, no. 5, pp. 845–851, 2004.

[6] M. Morrow, J. Waters, and E. Morris, "Mri for breast cancer screening, diagnosis, and treatment," *The Lancet*, vol. 378, no. 9805, pp. 1804–1811, 2011.

[7] S. M. Schoustra, R. Huijink, L. Alink, T. J. op't Root, D. Sprünken, D. Piras, W. F. M. Kobold, C. A. Klazen, M. C. van der Schaaf, F. M. van den Engh, W. Steenbergen, and S. Manohar, "The twente photoacoustic mammoscope 2: 3d vascular network visualization," in *Photons Plus Ultrasound: Imaging and Sensing 2019*, vol. 10878, p. 1087813, International Society for Optics and Photonics, 2019.

[8] R. A. Kruger, C. M. Kuzmiak, R. B. Lam, D. R. Reinecke, S. P. Del Rio, and D. Steed, "Dedicated 3d photoacoustic breast imaging," *Medical Physics*, vol. 40, no. 11, 2013.

[9] L. Lin, P. Hu, J. Shi, C. M. Appleton, K. Maslov, L. Li, R. Zhang, and L. V. Wang, "Single-breath-hold photoacoustic computed tomography of the breast," *Nature Communications*, vol. 9, no. 1, p. 2352, 2018.

[10] S. A. Ermilov, T. Khamapirad, A. Conjusteau, M. H. Leonard, R. Lacewell, K. Mehta, T. Miller, and A. A. Oraevsky, "Laser optoacoustic imaging system for detection of breast cancer," *Journal of biomedical optics*, vol. 14, no. 2, p. 024007, 2009.

[11] M. Xu and L. V. Wang, "Photoacoustic imaging in biomedicine," *Review of scientific instruments*, vol. 77, no. 4, p. 041101, 2006.

[12] S. Manohar and M. Dantuma, "Current and future trends in photoacoustic breast imaging," *Photoacoustics*, 2019.

[13] L. V. Wang and J. Yao, "A practical guide to photoacoustic tomography in the life sciences," *Nature methods*, vol. 13, no. 8, p. 627, 2016.

[14] J. Barcroft, *The respiratory function of the blood: Haemoglobin*. CUP Archive, 1928.

[15] P. Carmeliet and R. K. Jain, "Molecular mechanisms and clinical applications of angiogenesis," *Nature*, vol. 473, no. 7347, p. 298, 2011.

[16] M. Li, Y. Tang, and J. Yao, "Photoacoustic tomography of blood oxygenation: a mini review," *Photoacoustics*, vol. 10, pp. 65–73, 2018.

[17] S. Prahl, "Optical absorption of hemoglobin," 1999.

[18] B. T. Cox, J. G. Laufer, P. C. Beard, and S. R. Arridge, "Quantitative spectroscopic photoacoustic imaging: a review," *Journal of biomedical optics*, vol. 17, no. 6, p. 061202, 2012.

[19] M. Fonseca, B. Zeqiri, P. Beard, and B. Cox, "Characterisation of a phantom for multiwavelength quantitative photoacoustic imaging," *Physics in Medicine & Biology*, vol. 61, no. 13, p. 4950, 2016.

[20] M. Fonseca, B. Zeqiri, P. Beard, and B. Cox, "Characterisation of a pvcp based tissue-mimicking phantom for quantitative photoacoustic imaging," in *European Conference on Biomedical Optics*, p. 953911, Optical Society of America, 2015.

[21] E. Maneas, W. Xia, O. Ogunlade, M. Fonseca, D. I. Nikitichev, A. L. David, S. J. West, S. Ourselin, J. C. Hebden, T. Vercauteren, *et al.*, "Gel wax-based tissue-mimicking phantoms for multispectral photoacoustic imaging," *Biomedical optics express*, vol. 9, no. 3, pp. 1151–1163, 2018.

[22] W. C. Vogt, X. Zhou, R. Andriani, K. A. Wear, T. J. Pfefer, and B. S. Garra, "Photoacoustic oximetry imaging performance evaluation using dynamic blood flow phantoms with tunable oxygen saturation," *Biomedical optics express*, vol. 10, no. 2, pp. 449–464, 2019.

[23] M. Dantuma, R. C. van Dommelen, and S. Manohar, "A 3d semi-anthropomorphic photoacoustic breast phantom," in *Photons Plus Ultrasound: Imaging and Sensing 2019*, vol. 10878, p. 108781P, International Society for Optics and Photonics, 2019.

[24] M. Dantuma, R. C. van Dommelen, and S. Manohar, "A semi-anthropomorphic photoacoustic breast phantom," 2019.

[25] W. C. Vogt, C. Jia, K. A. Wear, B. S. Garra, and T. J. Pfefer, "Biologically relevant photoacoustic imaging phantoms with tunable optical and acoustic properties," *Journal of Biomedical Optics*, vol. 21, no. 10, p. 101405, 2016.

[26] C. Jia, W. C. Vogt, K. A. Wear, T. J. Pfefer, and B. S. Garra, "Two-layer heterogeneous breast phantom for photoacoustic imaging," *Journal of Biomedical Optics*, vol. 22, no. 10, p. 106011, 2017.

[27] Y. Lou, W. Zhou, T. P. Matthews, C. M. Appleton, and M. A. Anastasio, "Generation of anatomically realistic numerical phantoms for photoacoustic and ultrasonic breast imaging," *Journal of Biomedical Optics*, vol. 22, no. 4, p. 041015, 2017.

[28] H. Dehghani, B. W. Pogue, S. P. Poplack, and K. D. Paulsen, "Multiwavelength three-dimensional near-infrared tomography of the breast: initial simulation, phantom, and clinical results," *Applied Optics*, vol. 42, no. 1, pp. 135–145, 2003.

[29] E. L. Heffer and S. Fantini, "Quantitative oximetry of breast tumors: a near-infrared method that identifies two optimal wavelengths for each tumor," *Applied optics*, vol. 41, no. 19, pp. 3827–3839, 2002.

[30] N. Shah, A. Cerussi, C. Eker, J. Espinoza, J. Butler, J. Fishkin, R. Hornung, and B. Tromberg, "Noninvasive functional optical spectroscopy of human breast tissue," *Proceedings of the National Academy of Sciences*, vol. 98, no. 8, pp. 4420–4425, 2001.